PERGAMON

International Journal of Multiphase Flow 25 (1999) 827–840

International Journal of Multiphase Flow

www.elsevier.com/locate/ijmulflow

Water flow distribution in horizontal header contaminated with bubbles

Masahiro Osakabe *, Tomoyuki Hamada, Sachiyo Horiki

Tokyo University of Mercantile Marine, Koutou-Ku, Tokyo 135-8533, Japan

Received 12 July 1998; received in revised form 22 October 1998

Abstract

Flow headers for small multiple pipes are commonly used in boilers and heat exchangers. The system contributes to raise the heat transfer efficiency in the components. The flow distribution mechanism of the header for water has been studied and the calculation procedure for the design has been recommended for a single-phase condition. It is also recommended to avoid the bubbles in the header to obtain a uniform water flow rate to each small pipe, but in some cases, the header has to be used to distribute a flow containing bubbles. Distribution behavior of water with or without a gas-phase was studied experimentally in a horizontal header with four vertical pipes. The prediction method developed for a single-phase fluid was extrapolated to the flow containing bubbles. The prediction agreed well with the experimental results at a small amount of bubbles. © 1999 Elsevier Science Ltd. All rights reserved.

Keywords: Flow header; Multiple pipes; Boiler; Heat exchanger; Flow distribution; Bubbles; Prediction

1. Introduction

In boilers and heat exchangers, a horizontal header to distribute a fluid to multiple branch pipes is often used. The multiple branch pipes contribute to raise the heat transfer and thermal efficiency of the plants. The distribution mechanism is well understood and the guidelines for the header design have been established for a single phase flow (Kubo and Ueda, 1968). It is recommended to avoid the contamination of bubbles in the header to maintain uniform flow distribution to branch pipes because the bubble contamination significantly affects the flow distribution behavior in the header.

* Corresponding author.

0301-9322/99/$ - see front matter © 1999 Elsevier Science Ltd. All rights reserved.
PII: S0301-9322(98)00067-6

A condensation-type economizer of small boilers has been planned and developed to raise the thermal efficiency and decrease the emission of CO_2 (Osakabe, 1996). When the system does not include a deaerator, it is possible that some dissolved air in the feed water generates bubbles due to heating or local depressurization in the economizer. The knowledge of the header behavior when contaminated with bubbles is very important for the design of the heat exchanger system without a deaerator. The header is also used in the heat pump system for air conditioning of multiple rooms. As the thermal behaviors of evaporators or condensers are significantly affected by the refrigerant flow distribution in the header, the two-phase behavior in the header is also important.

The previous studies have been focused on a phase separation behavior at T-branches of piping (Hwang et al., 1988; Suu, 1988). Systematic study for the two-phase distribution to multiple branch pipes is scarce. Collier (1976) introduced the systematic study undertaken in Harwell but the detail has not been published. Watanabe et al. (1994) conducted a distribution experiment of two-phase flow in a horizontal header. Their result showed the contamination of gas-phase increased the liquid flow rates to the vertical branch pipes near the header inlet and reduced those far from the inlet at low liquid feed rates, but at high liquid feed rates, the liquid distribution rates to the inlet-side branch pipes decreased and those far from the inlet increased according to an increase of gas-phase. They also proposed a model to predict the two-phase distribution behavior in a horizontal header. Their model assumes all the liquid flows into a first inlet-side branch pipe at the initiation of gas contamination. Good predictions could not be obtained at the low gas flow rate.

Distribution behavior of water with or without a gas-phase was studied experimentally in a horizontal header with four vertical pipes. The prediction method developed for a single-phase fluid was extrapolated to the flow containing bubbles.

2. Experimental apparatus

Shown in Fig. 1 is a schematic diagram of the experimental apparatus. The apparatus consisted of a header, four vertical branch pipes and separators which were made of transparent acrylic resin for the observation of the flow pattern. The branch pipes were connected to the header at an interval of 130 mm. The entrance length between the header inlet and the first branch pipe was 600 mm to ensure a fully developed flow in the header. The length of the branch pipe could be varied as $h = 1000$, 800 and 585 mm to study the effect of length on the flow distribution. The cross-section of the header was 40×40 mm and the inner diameter of the branch pipes was $d = 10$ mm. The inner diameter and height of separator were 80 and 600 mm, respectively.

Water and air were supplied to the right side of header in the figure and distributed into branch pipes. The water and air were separated in the separators at the end of branch pipes and the water was collected. The water flow rate was obtained by noting the time interval to accumulate a known level of water in the separator. The air was released to atmosphere from the separator. The air flow rate supplied from a compressor was measured with an orifice or float-type flowmeters before entering the header.

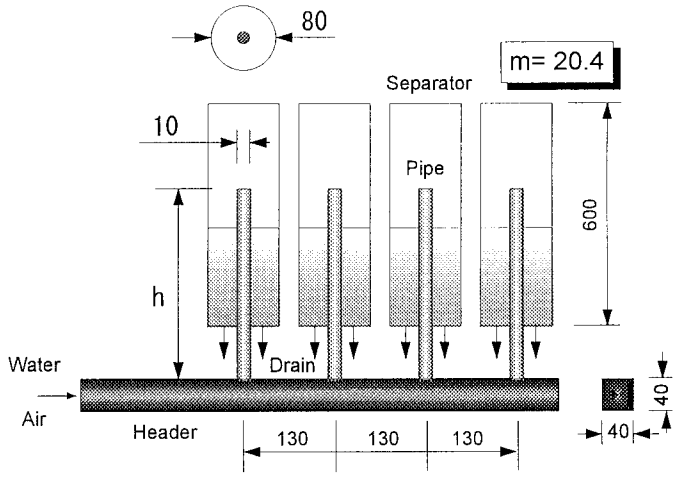

Fig. 1. Schematic of experimental apparatus.

3. Prediction method of water distribution

3.1. Single-phase flow

The header pressures before and after the branch pipe, i, counted from the header inlet are defined as P_i and P_{i+1}, respectively, as shown in Fig. 2. The ratio of the header flow area, A, to the branch pipe flow area, A_S, is defined as $m(=A/A_S)$. By using the pressure recovery coefficient, η, the pressure difference, $P_i - P_{i+1}$, is expressed as follows:

$$p_{i+1} - p_i = \eta \frac{\rho_L}{2}\left(j_{L,i}^2 - j_{L,i+1}^2\right) \tag{1}$$

where j is superficial velocity, ρ is density and a suffix L indicates water. It is reported that η is approximately 1 for the flow area ratio, m, of the present experimental apparatus and gradually decreases with a decrease in m (Kubo and Ueda, 1968). In the present calculation, η was fixed as 1 (refer to the Appendix).

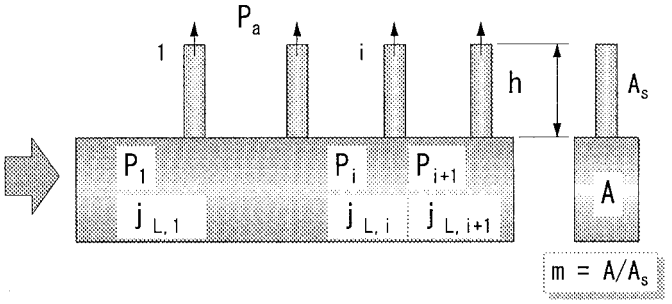

Fig. 2. Notation for calculation procedure.

The pressure difference between the inlet and outlet of the branch pipe is,

$$P_i - P_a = R\frac{\rho_L}{2}\left(j_{L,i} - j_{L,i+1}\right)^2 m^2 + \rho_L \mathbf{g} h \tag{2}$$

where $\mathbf{g}$ is acceleration due to gravity, h is branch pipe length and suffix "a" indicates atmosphere. The first term on the right-hand side is the pressure loss and the second one is the static pressure difference. The parameter, R, is a pressure loss coefficient defined as,

$$R = \xi + 4\lambda\frac{h}{d} \tag{3}$$

where d is the inner diameter of branch pipe. The inlet distribution loss coefficient, ξ, was assumed to be 0.5 in the present calculation. As a uniform distribution can be obtained with a larger value of R as mentioned below, 0.5 is used as a conservative value. The friction loss coefficient, λ, is defined as,

$$\lambda = 16/Re_S \qquad \text{for laminar flow,} \tag{4}$$

$$\lambda = 0.079 Re_S^{-0.25} \qquad \text{for turbulent flow,} \tag{5}$$

where Re_S is the Reynolds number in a branch pipe ($=u_S d/\nu_L$), u_S is water velocity in branch pipe and ν_L is the kinematic viscosity of water. The nondimensional pressure and velocity are defined as:

$$p_i^* = \frac{p_i - p_a - \rho_L \mathbf{g} h}{\rho_L j_{L,1}^2/2} \tag{6}$$

$$j_{L,1}^* = \frac{j_{L,i}}{j_{L,1}} \tag{7}$$

By using Eqs. (6) and (7), Eqs. (1) and (2) become:

$$p_{i+1}^* - p_i^* = \eta\left(j_{L,i}^{*2} - j_{L,i+1}^{*2}\right) \tag{8}$$

$$p_i^* = Rm^2\left(j_{L,i}^* - j_{L,i+1}^*\right)^2 \tag{9}$$

The above Eqs. (8) and (9) are the basic equations to give a flow distribution in the header. The important parameters in the equations are the flow area ratio, m, pressure recovery coefficient, η, and the pressure loss coefficient, R.

Shown in Fig. 3 is an iteration procedure to obtain the distributions of velocity and pressure in the header. The calculation starts at the velocity condition, $j_{L,1}^* = 1$ and an assumed pressure, P_1^*, at the header inlet. Eqs. (8) and (9) give the next nondimensional velocity and pressure in the header. This procedure yields the whole distribution of pressure and velocity in the header. After that, the assumed initial pressure is modified to give zero velocity in the

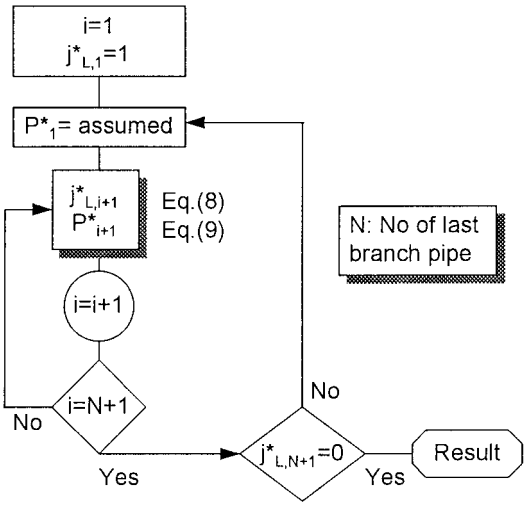

Fig. 3. Iteration procedure.

header just after the last branch pipe. The iteration is continued until zero velocity at the end of header is obtained.

The above calculation procedure gives the flow distribution rate into the branch pipes of different diameters, as shown in Fig. 4. In the calculation, the size of header and the number of branch pipes were the same as in the present experimental apparatus. The length of all the branch pipes was $h = 1000$ mm. The nonuniform distribution behavior can be observed for the pipes of $d = 30$ mm. The higher flow rate in the last pipe is due to the higher pressure in the header generated with the pressure recovery. By increasing the diameter of pipes, the flow rate to the inlet-side branch pipe decreased and that to the far end pipe increased. The uniform distribution was obtained for pipes of $d = 10$ mm which was used in the present experiment. The uniform distribution can be assured for pipes of smaller diameters corresponding to the larger flow area ratio, m.

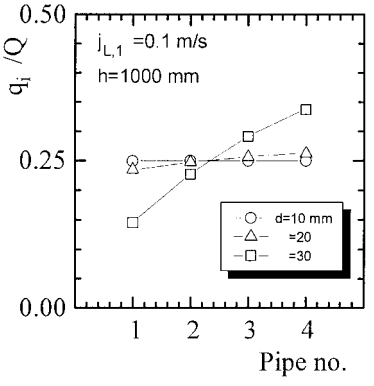

Fig. 4. Effect of pipe diameter for single-phase flow.

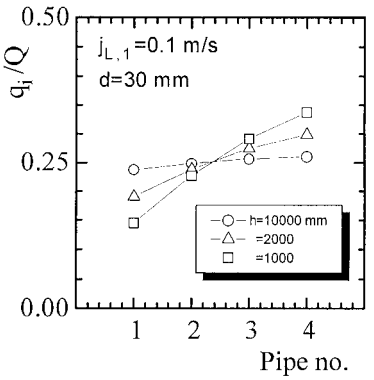

Fig. 5. Effect of pipe height for single-phase flow.

Fig. 4 shows a smaller flow rate to the inlet-side branch pipe than that to the end-side for the pipes of 30 mm diameter and 1000 mm length. In the model calculation, the pipe length, h, was increased to 2000 mm and 10000 mm, as shown in Fig. 5. The uniform flow distribution was obtained at the larger length of pipe. A uniform distribution can be assured at a larger pressure loss coefficient, R. The larger pressure loss in the branch pipe is also an important factor in obtaining a uniform distribution. So it is possible to be assured of uniform distribution by inserting orifices or valves to the branch pipes.

3.2. Contamination with a small amount of gas phase

Shown in Fig. 6 is a typical flow pattern observed in the header with a small amount of gas phase. The flow pattern at the header inlet was bubbly or stratified flow and the gas-phase was absorbed only into the first branch pipe. The flow pattern in the first branch pipe was a bubbly or slug flow. Considering the case of bubbly inlet flow, the pressure loss in the first branch pipe can be expressed as:

$$p_1 - p_a = R \cdot \frac{\rho_L}{2} \left(\frac{j_{L,1} - j_{L,2}}{1 - \alpha} \right)^2 m^2 + \rho_m \mathbf{g} h \tag{10}$$

where α is void fraction in the first branch pipe. In the above equation, the frictional pressure loss only takes account of the increase in water velocity due to the presence of bubbles. It is considered that the equation is appropriate when the amount of bubbles is relatively small. The

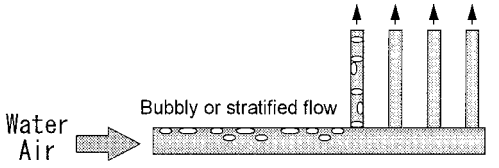

Fig. 6. Flow pattern with a small amount of gas phase.

average density of the two-phase mixture, ρ_m, is:

$$\rho_m = \alpha\rho_G + (1-\alpha)\rho_L \tag{11}$$

where the suffix "G" indicates air. The void fraction, α, can be obtained from the following drift flux model by Zuber and Findlay (1965), which is applicable to a wide range of volumetric flow rate in a pipe.

$$\alpha = \frac{j_{G,1}m}{1.13m\left(j_{G,1}+j_{L,1}-j_{L,2}\right)+1.18\left[\dfrac{\sigma(\rho_L-\rho_G)\mathbf{g}}{\rho_L^2}\right]^{1/4}} \tag{12}$$

where σ is surface tension. The nondimensional form of Eq. (10) by using Eqs. (6) and (7) is:

$$p_1^* = \frac{Rm^2\left(j_{L,1}^*-j_{L,2}^*\right)^2}{(1-\alpha)^2} - \frac{\alpha(\rho_L-\rho_G)\mathbf{g}h}{\rho_L j_{L,1}^2/2} \tag{13}$$

When the contamination of bubbles is relatively small, the effect of bubbles in the header was ignored in the present calculation. The pressure and velocity in the header were calculated with Eqs. (8) and (13) for the first branch pipe and with Eqs. (8) and (9) for the other pipes.

4. Experimental results and discussion

4.1. Single-phase flow

Shown in Fig. 7 is the relation between the header inlet *Re* number and the distribution flow rate to each pipe of different length. The distribution flow rate was approximately 0.25, indicating uniform distribution when *Re* is larger than 1500 ($j_{L,1}\approx 0.03$ m/s). When *Re* is relatively small, a nonuniform distribution was observed. Shown in Fig. 8 is the distribution flow rate to each pipe at $Re = 800$ ($j_{L,1}\approx 0.02$ m/s). These behaviors at *Re* less than 1500 are considered to be due to the flow instability in the distribution system. As the pressure in the header is considerably smaller at the low *Re* condition, the flow distribution can be strongly affected by the local effluent condition at the outlet of branch pipes. However, the prediction showed uniform distributions for each pipe of different length.

4.2. Contamination with a small amount of gas phase

The flow distribution experiment was conducted with the header inlet *Re* between 2000 and 4000 with a small amount of gas phase present in the header. In this range of *Re*, uniform distributions can be expected for the single-phase flow condition. Shown in Fig. 9 is the relation of water distribution rate to each pipe and the air velocity, $j_{G,1}$, at the water velocity, $j_{L,1}$, of 0.054 m/s. The solid and dashed lines are predictions for the distribution rates to the first pipe and the other pipes, respectively. The predicted flow rates to all the other pipes

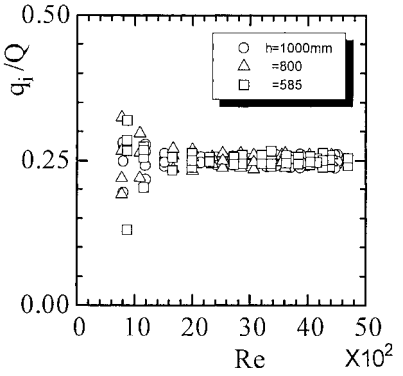

Fig. 7. Flow distribution for single-phase fluid.

except the first pipe were approximately the same. With a small amount of bubbles, the water distribution rate to the first pipe rapidly increases and the rates to the others decrease. As the bubbles in the header are absorbed only into the first pipe, the average two-phase density in the first pipe decreases. The decreased pressure head promotes the rush of water into the first pipe such as in an airlift pump. By increasing the air flow rate in the header inlet further, the flow rate to the first pipe takes a maximum and then tends to decrease. The increased air flow rate in the first pipe increases the pressure loss in the pipe and results in a reduction in the water flow rate. The more important behavior can be seen in the other pipes where the water flow rate decreases to one-fifth of the uniform distribution rate. The predictions agree well with the experimental results.

Shown in Fig. 10 is the relation of water distribution rate to each pipe and the air velocity, $j_{G,1}$, at the water velocity, $j_{L,1}$, of 0.085 m/s. Although the general behavior is the same as that observed in Fig. 9, the difference in water distribution rates between the first and the other pipes becomes smaller due to the increased water flow rate at the header inlet. The increased water flow reduces the void fraction and the airlift pump effect in the first branch pipe. The

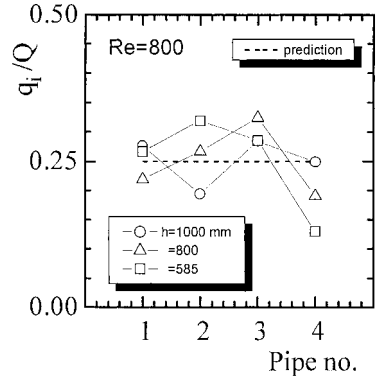

Fig. 8. Flow rate to each pipe at low flow rate.

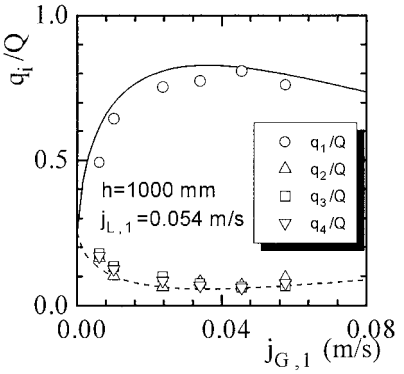

Fig. 9. Water flow distribution at $j_{L,1} = 0.054$ m/s.

water flow rate to the pipes except the first pipe decreases by as much as 40% of the uniform distribution rate. The predictions agree well with the experimental results also in this case.

Shown in Fig. 11 is the relation of water distribution rate to each pipe and the air velocity, $j_{G,1}$, at the water velocity, $j_{L,1}$, of 0.1 m/s. Although the general behavior is same as those observed in Figs. 9 and 10, the difference in water distribution rates between the first and the other pipes becomes smaller due to the increased water flow rate at the header inlet. The water flow rate to the pipes except the first pipe decreases by as much as 20% of the uniform distribution rate. The above results indicate the sufficient water supply to the header is necessary to ensure enough water to the pipes except the first pipe when the header is contaminated with a small amount of bubbles.

Shown in Fig. 12 is the effect of the pipe length, h, on the water distribution rates to the first pipe at $j_{L,1} = 0.066$ m/s. The solid, dashed and dot-dashed lines are predictions corresponding to $h = 1000$, 800 and 585 mm, respectively. Both the predictions and experiment show the larger water distribution rate to the first pipe with the larger pipe length. The larger distribution rate is considered to be due to the larger decrease in the static head in the longer pipe with the contamination of bubbles.

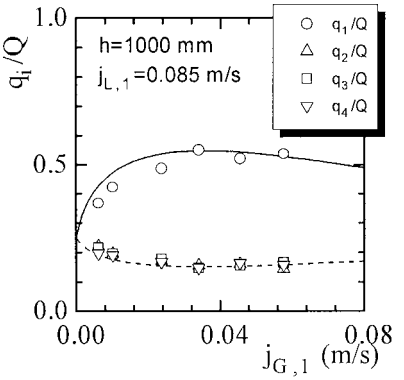

Fig. 10. Water flow distribution at $j_{L,1} = 0.085$ m/s.

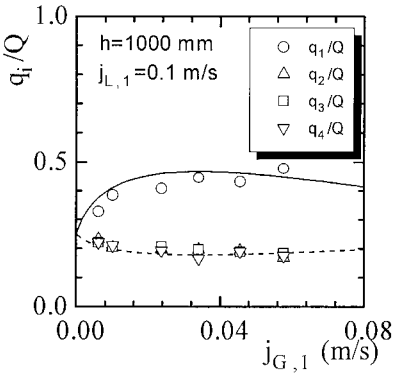

Fig. 11. Water flow distribution at $j_{L,1} = 0.1$ m/s.

Shown in Fig. 13 is the effect of the pipe length on the water distribution rate to the first pipe at $j_{L,1} = 0.085$ m/s. Although the general behavior is the same as that observed in Fig. 12, the maximum water distribution rate to the first pipe becomes smaller due to the increased water flow rate at the header inlet. Both the predictions and experimental results also show the larger water distribution rate with the larger pipe length. Although the larger length of pipe increases the flow resistance and assures a uniform distribution in a single phase flow, it promotes a nonuniform distribution with the contamination of bubbles. The larger pressure drop in the branch pipe is necessary for the uniform distribution. The above results for the increasing pipe length suggest the increase in the friction loss is relatively smaller than the decrease in the static head.

4.3. Contamination with a large amount of gas phase

Shown in Fig. 14 is a typical flow pattern observed in the header with a large amount of gas phase where $j_{G,1}$ is larger than 0.17 m/s. The flow pattern at the header inlet was stratified flow and the gas-phase was carried to not only the first pipe but also the other pipes. The gas flow

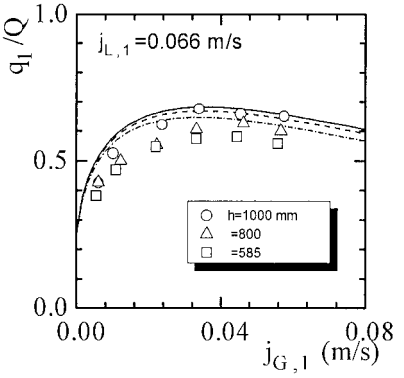

Fig. 12. Water flow rate to first pipe at $j_{L,1} = 0.066$ m/s.

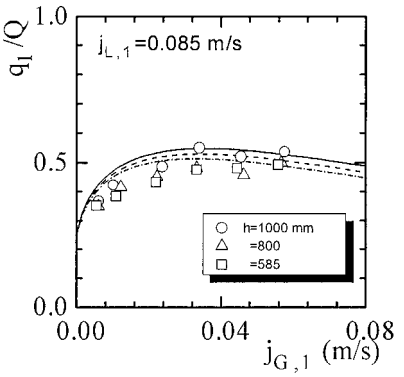

Fig. 13. Water flow rate to first pipe at $j_{L,1} = 0.085$ m/s.

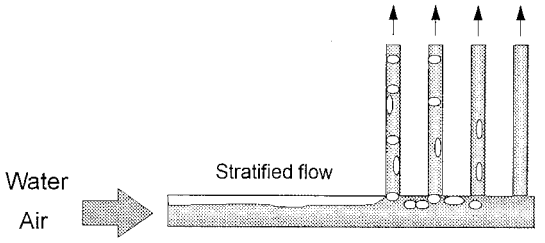

Fig. 14. Flow pattern with a large amount of gas phase.

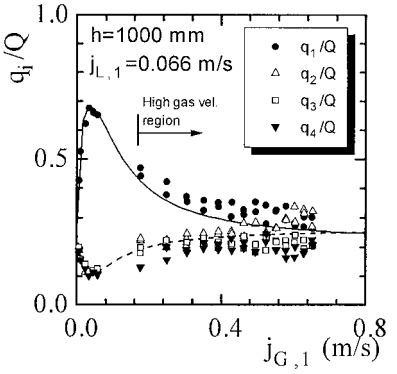

Fig. 15. Water distribution flow rate to each pipe at $j_{L,1} = 0.066$ m/s.

rate to the first pipe is seen to be the largest in the four pipes. The flow pattern in the vertical branch pipe was bubbly or slug flow.

Shown in Figs. 15–17 are the water distribution rate to each pipe including the data with a small amount of bubbles described above. Fig. 15 shows the water distribution rate at the header inlet velocity $j_{L,1}$ of 0.066 m/s. The water distribution rate to the first pipe increases to

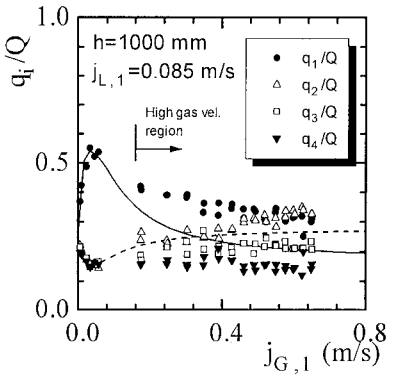

Fig. 16. Water distribution flow rate to each pipe at $j_{L,1} = 0.085$ m/s.

approximately 0.7 and that to the other pipes decreases to 0.1 at $j_{G,1} = 0.04$ m/s. By increasing the superficial air velocity further, the rate to the first pipe gradually decreases and that to the other pipes increases. All the experimental distribution rates approach a value of approximately 0.25, which is the uniform distribution rate. The solid and dashed lines are predictions assuming that the gas-phase flows only into the first pipe. At the region of high gas flow rate where $j_{G,1}$ is larger than 0.17 m/s, the predicted flow rate to the first pipe is slightly lower than the experimental results due to the carryover of gas-phase to the other pipes. However, the predictions for the first pipe and the others describe well the general experimental behavior.

Shown in Fig. 16 is the relation of water distribution rate to each pipe and the air velocity, $j_{G,1}$, at the water velocity, $j_{L,1}$, of 0.085 m/s. At the high gas flow rate, the prediction significantly underestimates the flow rate to the first pipe because the carryover of bubbles to the other pipes increases according to the increase in inlet water velocity. For more accurate predictions, the carryover mechanism should be studied further. The flow rate to the second pipe becomes approximately the same as that to the first pipe at $j_{G,1} = 0.65$ m/s. It should be noted that the rate to the fourth pipe is still the lowest, even at $j_{G,1} = 0.65$ m/s.

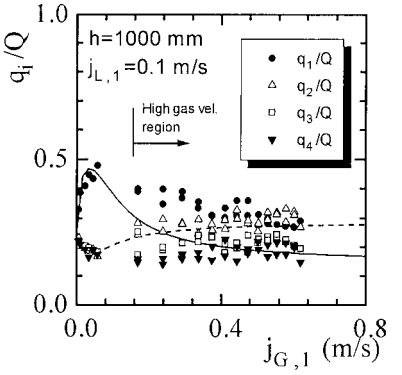

Fig. 17. Water distribution flow rate to each pipe at $j_{L,1} = 0.1$ m/s.

Shown in Fig. 17 is the relation of water distribution rates to each pipe and the air velocity $j_{G,1}$ at the water velocity $j_{L,1}$ of 0.1 m/s. Although the general behavior is the same as those observed in Fig. 16, the maximum water distribution rate to the first pipe becomes smaller due to the increased water flow rate at the header inlet. The flow rate to the second pipe becomes approximately the same as that to the first pipe at $j_{G,1} = 0.4$ m/s. The rate to the fourth pipe keeps the lower value even with a large amount of gas-phase. It is important that the distribution rates to the pipes at the high gas velocity are between the maximum and minimum rates predicted with the present model.

5. Conclusion

Distribution behavior of a water with or without gas-phase was experimentally studied in a horizontal header with four vertical branch pipes. The following major results were obtained:

1. When the *Re* in the header inlet was small, nonuniform distribution rates to branch pipes were observed even at a single-phase condition. This behavior at small *Re* less than 1500 is considered to be due to the flow instability in the distribution system.
2. With a contamination of a small amount of bubbles in the header, the water distribution rate to the first pipe rapidly increased and the rates to the others decreased. With the air flow rate increasing in the header inlet further, the flow rate to the first pipe took a maximum value and tended to decrease. A sufficient amount of water supply to the header was necessary to ensure enough water to all the pipes when the header was contaminated with a small amount of bubbles.
3. The larger length of pipe could ensure a uniform distribution in a single-phase flow, however, it promoted a nonuniform distribution in a header contaminated with a small amount of bubbles.
4. The prediction method developed for a single-phase fluid was extrapolated to the flow containing a small amount of bubbles. In the prediction, bubbles in the header were assumed to be completely absorbed into the first branch pipe. The prediction agreed well with the experimental results at a small amount of bubbles.
5. With the air velocity increasing further, the distribution rate to the first branch pipe gradually decreased and those to the other pipes tended to increase. The rates to the first and second pipes became approximately the same with a large amount of gas phase. However, the rate to the fourth pipe was kept to a lower value.

Appendix A

A momentum balance in a horizontal header with a mass effluent rate of m_S into the vertical branch pipe, as shown in Fig. A1, gives

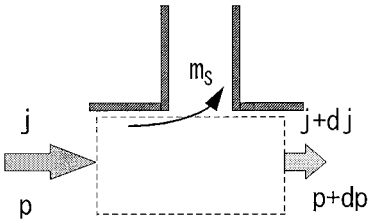

Fig. A1. Momentum balance in horizontal header.

$$\mathrm{d}p = \rho_{\mathrm{L}} j^2 - (\rho_{\mathrm{L}} j - m_{\mathrm{S}})(j + \mathrm{d}j) - m_{\mathrm{S}} j \tag{A1}$$

The third term on the right-hand side of Eq. (A1) takes account of the effluent rate of the horizontal momentum into the branch pipes. When only the vertical flow is allowed in the branch pipes, the effluent momentum term in the horizontal header should be zero. However, it is possible that the horizontal momentum can be carried into the branch pipe with a secondary flow in the pipe. By using $m_{\mathrm{S}} = -\rho_{\mathrm{L}}\,\mathrm{d}j$ and neglecting the higher-order small term, Eq. (A1) becomes

$$\mathrm{d}p = -\rho_{\mathrm{L}} j \mathrm{d}j \tag{A2}$$

By integrating Eq. (A2)

$$p_{i+1} - p_i = \frac{\rho_{\mathrm{L}}}{2}\left(j_{\mathrm{L},i}^2 - j_{\mathrm{L},i+1}^2\right) \tag{A3}$$

Eq. (A3) is equal to Eq. (1) with the pressure recovery coefficient $\eta = 1$. When the effluent momentum is $m_{\mathrm{S}} j$, the coefficient η becomes 1.

References

Collier, J.G., 1976. Single-phase and two-phase behaviour in primary circuit components. Proceedings of NATO Advanced Institute on Two-Phase Flow and Heat Transfer, 1. Hemisphere, Washington, DC, pp. 313–365.

Hwang, S.T., Soliman, H.M., Lahey, R.T., Jr, 1988. Phase separation in dividing two-phase flows. Int. J. Multiphase Flow 14, 439–458.

Kubo, T., Ueda, T., 1968. Study of header for flow distribution and concentration. Trans. JSME 34 (268), 2133–2138 (in Japanese).

Osakabe, M., 1996. Development of high-efficiency boiler. (in Japanese), NEDO report.

Suu, T., 1988. Air-water two-phase flow through a pipe junction (experiment on the local void fraction distribution adjacent to the branching part). Trans. JSME B54 (508), 3521–3526 (in Japanese).

Watanabe, M., Katsuta, M., Nagata, K., Sakuma, K., 1994. Two-phase flow distribution in multipass tube. Trans. JSME B60 (580), 4145–4150 (in Japanese).

Zuber, N., Findlay, J.A., 1965. Average volumetric concentration in two-phase flow systems. J. Heat Transfer 87, 453–468.